RSC Advances

ROYAL SOCIETY OF CHEMISTRY

www.rsc.org/advances

Reactivity of Carbon Black Diamond Electrode During the Electro-oxidation of Remazol Brilliant Blue R

Mohammed A. Ajeel, Mohamed Kheireddine Taeib Aroua*, Wan Mohd Ashri Wan Daud*

*** Department of Chemical Engineering, Faculty of Engineering, University of Malaya, 50603 Kuala Lumpur, Malaysia**

Email: mk_aroua@um.edu.my

Abstract

This article reports for the first time, the reactivity of Carbon Black Diamond (CBD) electrode using cyclic voltammetry and electrochemical impedance techniques in 0.25 M H_2SO_4 solution containing 0.5 mM $K_4Fe(CN)_6$. Three CBD electrodes with different contents of carbon black (5% (5CBD), 10% (10CBD), and 20% (20CBD) were used in this study. The reactions of the CBD electrodes had been quasi-reversible while 5CBD electrode performed the best activity compared to 10CBD and 20CBD electrodes. The anodic oxidation behavior of Remazol Brilliant Blue R (RBBR) was investigated by using cyclic voltammetry and electrochemical impedance techniques on the 5CBD electrode in different pH solution. The results indicated that the RBBR oxidized at 1.3 V, and the electro-oxidation process was more active at the low pH solution. Furthermore, the removal rate of RBBR on 5CBD attained 99.5% after 4 hour of the electro-oxidation process.

1. Introduction

Electrode material is one of the most important factors affecting the electrochemical oxidation process [1]. Many anode materials, such as F-doped PbO_2 [2], $Ti/Ru_{0.3}M_{0.7}O_2$ [3], β-PbO_2/α-PbO_2/Sb–SnO_2/TiO_2 [4], Er-chitosan-PbO_2 [5], and Pd/PPy/foam-Ni [6], Sn–Sb–Ni [7],

Ti/Sb–SnO2 [8, 9], and BDD [10, 11], have been tested and improved to use as anodes for electrochemical oxidation process of organic pollutant. Most previous studies have attempted to propose an efficient electrode with suitable electrochemical properties, long service life, and low cost. A carbon black diamond (CBD) electrode was proposed for the first time by our laboratory for organic pollutant oxidation. This electrode has an inert surface and suitable oxygen evolution potential that depended on the carbon black (CB) percentage in the electrode. The potential window for a CBD electrode with 5% CB is similar to that of a BDD electrode; however, increasing carbon black percentage, lead to decrease the potential window of CBD electrode [12]. Cyclic voltammetry and impedance techniques are used to investigate the electrochemical kinetic of the electrode. Redox reaction such as $K_3Fe(CN)_6/K_4Fe(CN)_6$, benzoquinone/hydroquinone, $Ce(NO_3)_3/Ce(NO_3)_4$ and $Ru(NH_3)^{3+/4+}$ have been used as probes to observe the change in behavior of electrode surface [13-15]. Cyclic voltammetry and electrochemical impedance techniques had been used by many researchers to characterize the electrochemical parameters for different electrodes [16], as well as to investigate the behavior of direct anodic oxidation of different organic pollutants, such as chlorophenols [17, 18], adenine [19], tetramethylthiourea [20], hydrazine and phenol [21]. Dyes and textile wastewater pose a serious environmental threat. Although, many researches have employed various techniques, such as direct and non-direct electrochemical oxidation, electro-Fenton, electro-coagulation, and other methods; very few have investigated the behavior of direct anodic oxidation of dyes via cyclic voltammetry or electrochemical impedance techniques. In this work, the effects of carbon black content and polytetrafluoroethylene binder on activities of diamond composite (CBD) electrode were investigated via cyclic voltammetry. Apart from that, electrode/electrolyte interface for CBD was investigated by using electrochemical impedance spectroscopy. Moreover, RBBR electro-oxidation on 5CBD electrode and its dependency on the main parameters, such as pH and initial concentration, were also investigated via cyclic voltammetry and electrochemical impedance spectroscopy methods. Also, RBBR electro-degradation was performed on 5CBD electrodes at different current density. RBBR was chosen as the model dye molecule for anodic oxidation with CBD because it is commonly used in textile industry.

2. Material and Method

2.1 Electrode Preparation:

Three disks of CBD electrode with three different content of carbon black (CB) 5%CB (5CBD), 10% CB (10CBD) and 20% CB (20CBD) have been prepared with surface area 1.1 cm^2. Whereas, diamond powder (98.3% purity and average particle size 6 nanometer, Sigma-Aldrich) was mixed carefully with a precise percent of carbon black (99% purity and average particle size of 13 nanometers, Alfa). Powder mixture have been mixed with suspension (60 wt%) in water (Sigma-Aldrich) polytetrafluoroethylene as the binder and 1,3- propanediol (98% purity, Sigma-Aldrich) and then dried as described in previous work [12]. In addition to the above mentioned method, electrodes were prepared but, without using polytetrafluoroethylene binder by press the mixed powders using piston pressing with 120Kg/cm^2.

2.2 Electrode Characterization:

2.2.1 Scanning electron microscopy analysis (SEM)

The morphological appearances of the CBD electrodes were studied by scanning electron microscopy (SEM) (Hitachi SU-8000, Japan) equipped with an energy-dispersive X-ray (EDX) analyzer. EDX determined the element content of the electrode.

2.2.2 Electrochemical Characterization of Electrode

Three CBD electrodes with different content of carbon black were investigated by cyclic voltammetry and electrochemical impedance technique to select the most efficient electrode for anodic oxidation of RBBR. EC-Lap sp-300 potentiostat with EC-Lap software V10.12 was used to perform the electrochemistry assays. Cyclic voltammetry runs were carried out in a single compartment, three-electrode system, which consisted of a CBD electrode as the working electrode, Ag/AgCl (3 M KCl) electrode as a reference electrode, and a platinum wire as counter electrode. The cyclic voltammetry runs of the CBD electrodes in a solution of 0.5 M H_2SO_4 containing 0.5 mM of $K_4Fe(CN)_6$ were recorded at different scan rate 20-100 mV/s. Klingler and Kochi [22] Eq.1 consider a suitable relation to estimate the electron transfer rate coefficient (k^o) for quasi-revisable reaction.

$$k^o = 2.18\sqrt{\frac{D\alpha n v F}{RT}}\ \exp[-(\frac{\alpha^2 nF}{RT})\ (E_p^{ox} - E_p^{red})] \quad (1)$$

where, k^o electron transfer rate coefficient, D diffusivity coefficient (6.2×10^{-4} cm^2/s) for $K_4Fe(CN)_6$, α is the transfer coefficient, n is the number of electrons transferred per mole. v is the scan rate (V/s), R is the gas constant (8.314 kJ/ K. mol), T is the absolute temperature (K), and $E_p^{ox} - E_p^{red}$ is the oxidation-reduction peaks separation potential.

The electrochemical impedance spectroscopy experiments were performed with a potential amplitude of the AC signal was kept at 10 mV and the measured frequency range was 0.01 –10^5 Hz.

2.3 Electrochemical Oxidation Behavior of Remazol Brilliant Blue R:

Voltammetric experiments were conducted in one compartment of a 100 mL glass cell at 25 °C to investigate the electrochemical oxidation behavior of RBBR (99.5% Sigma-Aldrich) on the 5CBD electrode (containing PTFE binder). A solution of 0.25 M H_2SO_4 (97% Merck Pro Analysis) as a blank solution, and three aqueous solutions of 600,400 and 100 mg/L of RBBR were prepared. The compositions of the solutions were 0.25 M H_2SO_4 at pH 1, 0.25 M Na_2SO_4 at pH 6.5 and 0.25 M KOH at pH 11. Milli-Q water was used to prepare the solutions. A platinum wire was used as the counter electrode, and Ag/AgCl was used as the reference electrode. EC-Lap sp-300 with EC-Lap software V10.12 potentiostat performed the electro-oxidation behavior on 5CBD electrode.

2.4 Electro-degradation of RBBR

An electrochemical cell with 100 mL of 100 mg/L RBBR, 0.25 M Na_2SO_4 as the supporting electrolyte was used for RBBR electro-degradation experiments on the 5CBD electrode. The experiments were conducted at applied current densities of 5, 10, or 15 mA/cm^2, and pH 3 at 25 °C temperature. ISO-TECH programmable power supply IPS 3202 was used, whereas stainless steel cathode and C-MAG HS 7 magnetic stirrer were used for solution mixing.

2.4.1 Analysis method

Chemical oxygen demand (COD) was analyzed by the standard method (HACH DRB 200). The concentrations of RBBR were determined by Lambda 35 UV-Vis spectrophotometer (PerkinElmer, U.S.A) at a wavelength of 590 nm. Prior to analysis, all the samples were filtered through a 0.22-μm filter membrane to eliminate the suspended solid that may affect the analysis process. The decomposition intermediates of RBBR during electrolysis was examined by high-performance liquid chromatography (HPLC) using an Agilent Technology 1200 series. C18 column (4.6 mm × 250 mm × 5μm) at 20℃ was used as the separation column. The eluent used was 60% acetonitrile/40% water (v/v); the injection volumes were 10 μL, and eluent flow rate was 1 mL/min. The detection wavelength was set at 254 nm.

3. Result and discussion

3.1 CBD Electrode Characterization

3.1.1 Morphology and structure characterization

SEM was used to investigate the morphology of carbon black diamond (CBD) composite electrodes. The scans were performed at high magnification (×50,000 times) with image resolution at 500 nm. The SEM images for 5CBD, 10BD, and 20CBD electrodes given in Fig. 1 clearly shows that a uniform topography, unique structure, and no separated carbon layers could be observed. Fig. 1(a) shows the SEM micrographs of the 5CBD electrode. It is obviously an excellent dispersion of the carbon black in the nanoparticles of the diamond. The composite particle grain size of 5CBD electrode was between 8 to 14 nm. Moreover, SEM micrographs show a homogenous distribution of Carbon black and diamond particles in the binder matrix. Fig 1(b) demonstrates a typical appearance of an agglomerate surface of the 10CBD electrode, which agglomerates consist of uniform porous particle matrix with an average grain size between 14 to 22 nm. SEM micrographs of the 20CBD electrode show a good dispersion of carbon black particles within the nanoparticles of the diamond and an average grain size between 13 to 30 nm as depicted in Fig 1(c). The porous morphology of CBD electrodes enhances the electrochemically active surface area of the electrodes, which lead to improving the electrodes reactivity.

The elements content in this electrode were determined by using SEM-EDX, and the spectrum are shown in Fig. 2. The CBD electrodes contained three types of elements, which are carbon (C), fluorine (F) and oxygen (O). C is the major element in this CBD electrodes with a nominal value of 78 % wt. F and O could be the element from the binder and solvent (polytetrafluoroethylene and 1,3- propanediol), the chemicals that have been used for electrode preparation.

3.1.2 Voltammetric Characterization:

The electrochemical performance of CBD electrode with three various percentages of carbon black (CB) had been evaluated via cyclic voltammetry method. Fig. 3 shows the electrochemical responses of CBD electrodes with 0.5 mM of $K_4Fe(CN)_6$ in 0.5 M H_2SO_4 at different scan rates (20, 50, and 100 mV/s). It was obvious the separation between anodic and cathodic peaks were more than 60/n mV and increase with scan rate, also the value of current peaks increase with the square root of scan rate. In addition, the cathodic peak shifts to a negative value with increase the scan rate. These criteria lead to conclude the reactions on the three different CBD electrodes have been quasi-reversible [23-25]. Besides, the separation between anodic and cathodic potential peaks for 5CBD, 10CBD, and 20CBD electrodes were 220-422 mV, 249-455 mV, and 253-458 mV at scan rates 20-100 mV/s respectively. According to Klingler and Kochi relationship [22] Eq. (1), the charge-transfer reaction rate constant k^o values have been estimated. Results show the k^o of 5CBD, 10CBD, and 20CBD electrodes were 3.95×10^{-4}, 2.63×10^{-4}, and 2.57×10^{-4} cm/s respectively. However, the rate of electron transfer between the solution and the 5CBD electrode was faster than those of 10CBD and 20CBD electrodes. For same redox couple, the CBD electrodes results are congruent with that of boron doped diamond electrodes, where k^o values are reported to vary from 10^{-2} to 10^{-5} cm/s [23, 26-29]. On top of that, the peak-peak potential separation of the CBD electrodes had been so close to that of as-grown BDD electrode [30]. Also, the separation between anodic and cathodic potential peak on CBD was higher than that registered on BDD electrode, which is attributed to the presence of PTFE particles in CBD composition. Besides, it is well-known that the nonconductive particles on electrode surface reduced its activity while the amount and the type of binder had a significant effect on electrode activity [31]. Thus, to verify this

hypothesis, three electrodes; 5CBD, 10CBD, and 20CBD, were prepared without using the PTFE binder. Cyclic voltammetry results for these electrodes marked a reduction in the anodic and cathodic peak potential separation with significant amounts as depicted in Fig. 4. Also, the k^o became higher with 6.88×10^{-4}, 3.15×10^{-4}, and 2.94×10^{-4} cm/s for 5CBD, 10CBD, and 20CBD electrodes respectively. That revealed that the PTFE binder has a significant effect on electrode activity. Although the increase of the binder percent led to producing a composite electrode with high hardness, it reduced the electron transfer rate between the electrode and the solution.

3.1.3 Electrochemical Impedance Characterization:

Electrochemical impedance spectroscopy is one of the most efficient techniques used to investigate the electrochemical parameters of electrode/electrolyte interface [32, 33]. Potassium ferrocyanide of 5mM in 0.5 M H_2SO_4 had been selected as a probe with the potential of 0V vs. Ag/AgCl, as well as a frequency range of $0.01–10^5$ Hz to evaluate the performance of CBD electrodes. Fig. 5 shows the Nyquist plot for 5CBD, 10CBD, and 20CBD electrodes. A semicircle was observed at high frequencies, whereas a straight line with a unit slope was found for low frequencies, which revealed the kinetic and the mass transfer control respectively [34]. Also, the best fit for CBD electrodes impedance spectra were the Randles equivalent circuit, as shown in the inset of fig. 5. The fitting parameters consisted of the solution resistance (R_s), which was in parallel with a combination of the impedance of the faradic reaction and double layer capacitance (C_{dl}). Other than that, faradic reaction impedance consisted of charge transfer resistance (R_{ct}), together with Warburg resistance (W) [35-37]. Warburg impedance is a mass transfer resistance for redox species during diffusion from and to electrode surface [38]. Meanwhile, the diameter of the semicircle represents the values of R_{ct} and from Fig. 5, it is obvious that this value on 5CBD electrode has been the least. Whereas, the R_{ct} were 1.99 Ω cm^2, 6.4 Ω cm^2, and 11.49 Ω cm^2 on 5CBD, 10CBD, and 20CBD electrodes respectively. In contrary, among the values retrieved from double layer capacitance, 5CBD displayed the highest value in comparison to those obtained from 10CBD and 20CBD. Hence, the increase in double layer capacitance and the decrease in charge transfer resistance indicated that there was an increased density of ionic charges at the electrode/electrolyte interface [39]. Indeed, the

small values of capacitance within 1 μF cm^{-2} for the three electrodes were attributed to the space charge layer caused by the semi-metal character of CBD electrodes [40]. These values of CBD electrodes with double-layer capacitance were low and had been similar to BDD electrode capacitance, which was ten times lower than glassy carbon electrode capacitance [41, 42]. Thus, based on the above values of charge transfer resistance, it can be concluded the electron transfer rate on 5CBD was easier than on 10CBD and 20CBD electrodes. So the electrochemical activity of 5CBD was higher than 10CBD and 20CBD electrodes [43]. Impedance results were congruent with that of cyclic voltammetry. Whereby in both techniques, the effect of increased CB content in CBD electrodes led to the reduction in the electrochemical activity of the electrode.

3.2 Remazol Brilliant Blue R Anodic Oxidation

3.2.1 Cyclic Voltammetry:

Cyclic voltammetry approach was used to study the anodic oxidation of RBBR behavior on 5CBD electrode, as shown in fig. 6(a). The cyclic voltammetry method was used to investigate at a 0.1 V/s scan rate in solutions of 0.25 M H_2SO_4 (pH 1) in the absence and the presence of 400 mg/L of RBBR. The scanning was performed towards the oxidation direction from -0.1 to 1.8V. The oxidation peak potentials were observed at 1.3 V vs. Ag/AgCl, and no reduction peak appeared, which revealed that the anodic oxidation of RBBR on 5CBD electrode was irreversible. Besides, the value of anodic current peaks reduced considerably with further runs, while, after 8 runs, the current oxidation peaks became stable and did not change or disappear. Fig. 6(b) shows the cyclic voltammetry of 400 mg/L for RBBR on 5CBD electrode with different scan rates at 20, 50, 75, 100, and 200 mV/s. The oxidation potential peaks, as well as the current peaks, increased with the increasing potential scan rates. Moreover, the peak potentials were shifted to a positive direction, which revealed that the RBBR electrochemical oxidation was totally irreversible [44, 45]. Furthermore, the plots of the anodic current peaks versus the square roots of the scan rate showed a straight line. So, it can be concluded that the electrochemical oxidation of RBBR on 5CBD electrode was a diffusion controlled process. Besides, to study the effect of pH value on electro-oxidation behavior of 400 mg/L RBBR. A neutral solution of 0.25 M Na_2SO_4 (pH 6.5) and base solution of 0.25 M

KOH (pH 11) were selected to compare with the behavior of RBBR electro-oxidation in acid solution. Fig. 7(a) shows that the anodic oxidation peak in acid solution was the highest compared to the neutral and the base media. Hence, it was obvious that the electro-oxidation of RBBR on 5CBD electrode favored the acid solution. This result is found to be congruent with electrochemical oxidation of RBBR on BDD and DSA electrodes[46-48]. Three different concentrations verified the effect of RBBR concentration on the anodic oxidation process. Fig. 7(b) shows the voltammogram of 600, 400, and 100 mg/L of RBBR in an acidic aqueous solution of 0.25 M H_2SO_4, and 100 mV/s scan rate. Thus, it has been obvious that the increase in the concentration of RBBR led to the increase of oxidation current peak. On the other hand, there was an insignificant change in oxidation potential peak values with the increase in RBBR concentration. It might be associated with the same electro-oxidation kinetics for the various RBBR concentrations [49]. Plus, reduction of oxidation current peak with reduced the RBBR concentration might be attributed to the conversion of oxidation process from charge transfer controlled at high concentration to mass transfer controlled at low concentration [50].

3.2.2 Electrochemical Impedance:

The electrochemical impedance spectra of RBBR electro-oxidation on 5CBD electrode were investigated in the frequency region between 50 and 10^5 Hz. The narrow frequency range, particularly in the low frequency region, had been selected to avoid nonstationary in the system, especially with high potential. Most electrochemical systems show some nonstationary behavior due, for example, to the growth of surface films on the electrode, and its consider one of the Bias errors happen during impedance measurement, which result from a substantial change in the system [51]. Whereas, the application of high potential led to the continuous formation of a polymeric passive film on electrode surface [52, 53] during RBBR oxidation process. The spectra of the RBBR oxidation were registered by a various applied potential with an interval between 0.6 and 1.9 V for an aqueous solution of 0.25 M H_2SO_4 contain 400mg/L of RBBR. Fig. 8 shows various shapes of impedance plots, whereas the value of capacitive loops increased with applied potential until it reached the maximum value at 1.3V. The subsequent capacitive loops were reduced with applied potential and became minimum at 1.9V. Moreover, depending on

the applied potential, the fitting for the spectra was divided into two equivalent circuits. At the applied potential, which led to oxidizing RBBR (0.8 – 1.5 V), the suitable fit for the spectra had been the equivalent circuit, as shown in Fig. 9(a). Whereas, R_s represented the solution resistance; double layer capacitance, C_{dl}; charge transfer (passivation) resistance, R_{ct}; adsorption capacitance of the reaction intermediates, C_{ads}; and the resistance imposed by the reaction intermediates adsorbed at the electrode surface, R_{ads}. As for the impedance at an applied potential where there was no oxidation of RBBR occurred (1.7 – 1.9 V), the best fit for the spectra was the equivalent circuit, as portrayed in Fig. 9(b). The difference in the equivalent circuits of the system attributed to the deviation that took place at the electrode/electrolyte interface. Indeed, the electro-oxidation of RBBR produced of intermediate compounds that adsorbed on the electrode surface, which led to producing a totally different interface with new components (R_{ads} and C_{ads}). Based on the values of spectra, as depicted in Fig. 8, and charge transfer resistance, as listed in Table 1, it could be concluded that the oxidation potential of RBBR was at 1.3V. Nevertheless, the formation of the intermediate compounds during the RBBR electro-oxidation caused the blocking of the electrode surface and maximized the size of the spectra. This result confirms the result of cyclic voltammetry in part 3.2.1. Charge transfer resistance values were reduced at applied potential higher than 1.3 V as the potential was close to oxygen evolution potential, particularly at 1.9 V [54]. Moreover, Table 1 depicts that the value of charge transfer resistance is higher than adsorption resistance, which means, the charge transfer resistance dominated the electrode kinetics under experimental condition[55]. With the same procedure, the oxidation potential of RBBR on 5CBD electrode in an aqueous solution of 0.25 M Na_2SO_4 (pH 6.5) and 0.25 M KOH (pH 11) had been measured. Furthermore, the maximum spectra diameter registered in 0.25 M Na2SO4 (pH 6.5) and 0.25 M KOH (pH 11) were at 1.25 V and 1.1 V respectively. Fig. 10(a) illustrates the impedance plots for electro-oxidation of 400 mg/L RBBR on 5CBD electrode concerning oxidation potential for three different supported electrolytes. Also, the impedance plots at applied potential zero V for the same electrodes and electrolytes are shown in Fig. 10(b). Even, it had been easy to observe the deviation in the impedance between two applied potentials. However, the behavior of 5CBD at three different electrolytes shared similar trends at both applied potentials. The

values of spectra plots in both potentials had been the highest in KOH solution while less in Na_2SO_4 and H_2SO_4 respectively. Which marked the electro-oxidation of RBBR on 5CBD that favored the acid, and this had been in agreement with the results obtained by the cyclic voltammetry technique. Meanwhile, from a comparison of the deviation in the impedance plots depicted in Fig. 10 for both applied potentials, it had been easy to exhibit the effect of passivation phenomenon on electrode/electrolyte interface for the three different pH solutions. Moreover, the fit of equivalent circuits changed from Randles equivalent circuit at zero V of applied potential, such as those described in the inset of Fig 5, to a more complex circuit, as in Fig. 9(a), for impedance at oxidation potential. Plus, in order to investigate the passivation phenomenon of the 5CBD electrode in a solution of 400 mg/L, the RBBR. Impedance runs with consecutive scan was performed at each oxidation potential for the three different pH solutions (pH 1, pH 6.5, and pH 11). Fig. 8 shows the significant increase in the spectra sizes with successive scans, revealing the effect of electrode surface blocking on the values of charge-transfer resistance. As expected, the maximum passivation occurred at a higher pH solution. Thus, this might be a significant parameter that made the electro-oxidation reactivity of RBBR on the 5CBD electrode surface be the least at the base medium and the highest in an acidic medium.

3.3 Electro-degradation of RBBR

The electrochemical incineration of 100 mg/L of RBBR at 25℃ temperature, 0.25 M Na_2SO_4 as supporting solution, and current density 5-15 mA/cm^2 was investigated on the 5CBD electrode. According to the result of impedance, the aqueous solution of pH 3 was selected for the electro-degradation process. Fig. 12(a) shows the electro-degradation of 100 mg/L RBBR. After 4 hour of reaction, the RBBR removal efficiencies of 99.5%, 97%, and 88%, were respectively obtained at 15, 10, and 5 mA/cm^2. Fig. 11(b) shows the COD decay through anodic oxidation: COD removal efficiencies of 66%, 54%, and 45% were respectively obtained at 15, 10, and 5 mA/cm^2. These results correspond with previous results on reductions in RBBR concentration. The COD decay efficiency is lower than the RBBR removal efficiency because of accumulation of electro-degradation products. Aliphatic acids mainly oxalic acid and malic acid were the primary

intermediates with a tiny amount of benzene and benzoquinone; HPLC determined these products. The applied current density is a key operating consideration in electro-oxidation of organic pollutants because this factor influences the amount of reactive hydroxyl radicals generated at the anode [56]. Fig. 12(b) shows the RBBR degradation rate and COD decay apparently increased with the current density. These results reveal that degradation of 100 mg/L RBBR is controlled by charge transfer because a greater charge passing through the cell leads to oxidation of RBBR and its intermediates [57]. However, although increases in current density can reduce the time required to oxidize the pollutant electrochemically, it also reduces the electrode current efficiency [58]. According to the result reported by D. Montanaro and E. Petrucci[48], the discolouration of 50 mg/L of RBBR on BDD electrode at 30 mA/cm^2 was observed after 260 min. Hence it is clearly from the above results, the removal rate of RBBR on 5CBD electrode was faster than that on BDD electrode.

4. Conclusions

Increase in carbon black percentage in CBD electrodes reduced the values of activity in the electrode, whereas the anodic and cathodic potential separation peak increased with carbon black content. On the other hand, the charge transfer resistance value of CBD electrodes also increased with higher carbon black percentage, which revealed the decline in the rate of electrode reactivity. Moreover, 5CBD was registered as the best electrochemical parameter compared to 10CBD and 20CBD electrodes, whereby the values of peak potential separation and charge transfer resistance were the lowest for 5CBD electrode. Besides, the behavior of anodic oxidation of RBBR on 5CBD electrode was investigated via cyclic voltammetry and electrochemical impedance techniques in acidic, neutral, and base aqueous solutions. The anodic oxidation current peaks in acidic solution were the highest. While the charge transfer resistance had been the lowest compared to those in neutral and base solutions, which revealed that the anodic oxidation of RBBR on 5CBD was more active at the low pH solution. On the other hand, the passivation of the 5CBD electrode during RBBR oxidation was the highest at a high pH solution. Furthermore, RBBR degradation rates increased with increasing current density.

Acknowledgement

This work was carried at the Center for Separation Science and Technology (CSST) and was financed through the High Impact Research Grant Project No. UM.C/HIR/MOE/ENG/43.

References

1. P. Actis, A. Denoyelle, R. Boukherroub and S. Szunerits, *Electrochemistry Communications*, 2008, **10**, 402-406.
2. J. Cao, H. Zhao, F. Cao, J. Zhang and C. Cao, *Electrochimica Acta*, 2009, **54**, 2595-2602.
3. R. Coteiro and A. De Andrade, *Journal of Applied Electrochemistry*, 2007, **37**, 691-698.
4. J. Wu, H. Xu and W. Yan, *RSC Advances*, 2015, **5**, 19284-19293.
5. Y. Wang, Z. Shen and X. Chen, *Journal of hazardous materials*, 2010, **178**, 867-874.
6. Z. Sun, H. Ge, X. Hu and Y. Peng, *Separation and Purification Technology*, 2010, **72**, 133-139.
7. Y. Wang, K. Chan, X. Li and S. So, *Chemosphere*, 2006, **65**, 1087-1093.
8. D. Shao, X. Li, H. Xu and W. Yan, *RSC Advances*, 2014, **4**, 21230-21237.
9. Y.-H. Cui, Q. Chen, J.-Y. Feng and Z.-Q. Liu, *RSC Advances*, 2014, **4**, 30471-30479.
10. P. Canizares, J. Garcia-Gomez, C. Saez and M. Rodrigo, *Journal of applied electrochemistry*, 2003, **33**, 917-927.
11. M. Rodrigo, P. Michaud, I. Duo, M. Panizza, G. Cerisola and C. Comninellis, *Journal of the Electrochemical Society*, 2001, **148**, D60-D64.
12. M. A. Ajeel, M. K. Aroua and W. M. A. W. Daud, *Electrochimica Acta*, 2015, **153**, 379-384.
13. I. Duo, A. Fujishima and C. Comninellis, *Electrochemistry Communications*, 2003, **5**, 695-700.
14. A. Polcaro, P. Ricci, S. Palmas, F. Ferrara and A. Anedda, *Thin solid films*, 2006, **515**, 2073-2078.
15. E. Guinea, F. Centellas, E. Brillas, P. Cañizares, C. Sáez and M. A. Rodrigo, *Applied Catalysis B: Environmental*, 2009, **89**, 645-650.
16. F. Marken, C. A. Paddon and D. Asogan, *Electrochemistry communications*, 2002, **4**, 62-66.
17. L. Pigani, M. Musiani, C. Pirvu, F. Terzi, C. Zanardi and R. Seeber, *Electrochimica acta*, 2007, **52**, 1910-1918.
18. C. Berrios, R. Arce, M. Rezende, M. Ureta-Zanartu and C. Gutierrez, *Electrochimica Acta*, 2008, **53**, 2768-2775.
19. C. Berríos, J. F. Marco, C. Gutiérrez and M. S. Ureta-Zañartu, *Electrochimica Acta*, 2009, **54**, 6417-6425.
20. A. Bolzán and L. Gassa, *Journal of Applied Electrochemistry*, 2014, **44**, 279-292.
21. H. Karimi-Maleh, M. Moazampour, A. A. Ensafi, S. Mallakpour and M. Hatami, *Environmental Science and Pollution Research*, 2014, **21**, 5879-5888.
22. R. Klingler and J. Kochi, *The Journal of Physical Chemistry*, 1981, **85**, 1731-1741.
23. N. G. Ferreira, L. L. G. Silva, E. J. Corat and V. J. Trava-Airoldi, *Diamond and Related Materials*, 2002, **11**, 1523-1531.
24. J. Zang, Y. Wang, S. Zhao, L. Bian and J. Lu, *Diamond and related materials*, 2007, **16**, 16-20.

25. B. Ntsendwana, B. B. Mamba, S. Sampath and O. A. Arotiba, *RSC Advances*, 2013, **3**, 24473-24483.
26. A. Modestov, Y. E. Evstefeeva, Y. V. Pleskov, V. Mazin, V. P. Varnin and I. Teremetskaya, *Journal of Electroanalytical Chemistry*, 1997, **431**, 211-218.
27. J. Xu, Q. Chen and G. M. Swain, *Analytical Chemistry*, 1998, **70**, 3146-3154.
28. V. Fisher, D. Gandini, S. Laufer, E. Blank and C. Comninellis, *Electrochimica acta*, 1998, **44**, 521-524.
29. S. Ferro and A. De Battisti, *Electrochimica Acta*, 2002, **47**, 1641-1649.
30. G. M. Swain and R. Ramesham, *Analytical chemistry*, 1993, **65**, 345-351.
31. L. Fransson, T. Eriksson, K. Edström, T. Gustafsson and J. O. Thomas, *Journal of power sources*, 2001, **101**, 1-9.
32. C. M. Brett, A. O. Brett and P. Electrochemistry, *Journal*, 1993.
33. S. C. B. Oliveira and A. M. Oliveira-Brett, *Electrochimica Acta*, 2010, **55**, 4599-4605.
34. X.-Z. R. Yuan, C. Song, H. Wang and J. Zhang, *Electrochemical impedance spectroscopy in PEM fuel cells: fundamentals and applications*, Springer Science & Business Media, 2009.
35. A. Sakharova, L. Nyikost and Y. Pleskov, *Electrochimica acta*, 1992, **37**, 973-978.
36. J. Hernando, S. Q. Lud, P. Bruno, D. M. Gruen, M. Stutzmann and J. A. Garrido, *Electrochimica Acta*, 2009, **54**, 1909-1915.
37. Z. Bo, Z. Wen, H. Kim, G. Lu, K. Yu and J. Chen, *Carbon*, 2012, **50**, 4379-4387.
38. S. Hwang, B. S. Lee, Y. S. Chi, J. Kwak, I. S. Choi and S.-g. Lee, *Electrochimica Acta*, 2008, **53**, 2630-2636.
39. X. Tong, M. Liu and G. Zhao, *Journal of Solid State Electrochemistry*, 2010, **14**, 221-224.
40. E. Mahé, D. Devilliers and C. Comninellis, *Electrochimica acta*, 2005, **50**, 2263-2277.
41. X. Zhu, M. Tong, S. Shi, H. Zhao and J. Ni, *Environmental science & technology*, 2008, **42**, 4914-4920.
42. M. Hupert, A. Muck, J. Wang, J. Stotter, Z. Cvackova, S. Haymond, Y. Show and G. M. Swain, *Diamond and Related Materials*, 2003, **12**, 1940-1949.
43. Y. Liu, H. Liu, J. Ma and J. Li, *Journal of hazardous materials*, 2012, **213**, 222-229.
44. T. Mafatle and T. Nyokong, *Analytica Chimica Acta*, 1997, **354**, 307-314.
45. J. Xavier, E. Ortega, J. Ferreira, A. Bernardes and V. Pérez-Herranz, *Int. J. Electrochem. Sci*, 2011, **6**, 622-636.
46. A. H. Degaki, G. F. Pereira, R. C. Rocha-Filho, N. Bocchi and S. R. Biaggio, *Electrocatalysis*, 2014, **5**, 8-15.
47. D. Rajkumar, B. J. Song and J. G. Kim, *Dyes and pigments*, 2007, **72**, 1-7.
48. D. Montanaro and E. Petrucci, *Chemical Engineering Journal*, 2009, **153**, 138-144.
49. X. Duan, L. Tian, W. Liu and L. Chang, *Electrochimica Acta*, 2013, **94**, 192-197.
50. C. Comninellis and G. Chen, *Electrochemistry for the Environment*, Springer, 2010.
51. M. E. Orazem and B. Tribollet, *Electrochemical impedance spectroscopy*, John Wiley & Sons, 2011.
52. L. Pigani, M. Musiani, C. Pirvu, F. Terzi, C. Zanardi and R. Seeber, *Electrochimica Acta*, 2007, **52**, 1910-1918.
53. X.-M. Wang, J.-M. Hu, J.-Q. Zhang and C.-N. Cao, *Electrochimica Acta*, 2008, **53**, 3386-3394.
54. B. Pierozynski, T. Mikolajczyk and G. Piotrowska, *Int. J. Electrochem. Sci*, 2015, **10**, 2432-2438.
55. W. Yang, W. Yang and X. Lin, *Applied Surface Science*, 2012, **258**, 5716-5722.
56. A. El-Ghenymy, J. A. Garrido, R. M. Rodríguez, P. L. Cabot, F. Centellas, C. Arias and E. Brillas, *Journal of Electroanalytical Chemistry*, 2013, **689**, 149-157.

57. J. Y. Choi, Y.-J. Lee, J. Shin and J.-W. Yang, *Journal of hazardous materials*, 2010, **179**, 762-768.
58. J. Czupryniak, A. Fabiańska, P. Stepnowski, T. Ossowski, R. Bogdanowicz, M. Gnyba and E. M. Siedlecka, *Central European Journal of Physics*, 2012, **10**, 1183-1189.

Figure caption

Figure 1. Scanning electron microscopy (SEM) images for (a) 5CBD electrode, (b) 10CBD electrode, and (c) 20CBD electrode.

Figure 2. SEM-EDX spectrum for (a) 5CBD electrode, (b) 10CBD electrode, and (c) 20CBD electrode.

Figure 3. Cyclic voltammograms of 5CBD, 10CBD and 20CBD electrodes in aqueous solution of 0.5 M H_2SO_4 containing 5mM $K_4Fe(CN)_6$ at different scan rate (20, 50, and 100 mV/s) and 25 ^{0}C.

Figure 4. Cyclic voltammograms of 5CBD, 10CBD, and 20CBD electrodes content without PTFE binder in aqueous solution of 0.5 M H_2SO_4 containing 5mM $K_4Fe(CN)_6$ at 100 mV/s scan rate and 25 ^{0}C.

Figure 5. Nyquist plot of 5CBD, 10CBD and 20CBD electrodes in aqueous solution of 0.5 M H_2SO_4 containing 5mM $K_4Fe(CN)_6$ at zero potential vs. Ag/AgCl. Inset is the equivalent circuit used in the fitting of the Nyquist plots.

Figure 6. Cyclic voltammetry curves of 5CBD electrode (a) in blank aqueous solution of 0.25 M H_2SO_4 and aqueous solutions of 0.25 M H_2SO_4 (pH 1) containing 400 mg/L RBBR at a scan rate 100 mV/s and 25℃ temperature (b) at different scan rates 20, 50, 70, 100 and 200 mV/s. Inset plot is the current peaks vs. square root of scan rate.

Figure 7. Cyclic voltammetry curves of 5CBD electrode in (a) aqueous solution of 0.25 M H_2SO_4 (pH 1), 0.25 M Na_2SO_4 (pH 6.5) and 0.25 M KOH (pH 11) containing 400

mg/L RBBR at scan rate 20 mV/s. (b) Aqueous solution of 0.25 M H_2SO_4 (pH 1), containing 600,400 and 100 mg/L RBBD at scan rate 100 mV/s and 25℃ temperature.

Figure 8. Nyquist plots of the 5CBD electrode in an aqueous solution of 0.25 M H_2SO_4 containing 400 mg/L RBBR at different applied potential and 25℃ temperature.

Figure 9. Equivalent circuits used in the fitting of the Nyquist plots of the 5CBD electrode in an aqueous solution of 0.25 M H_2SO_4 containing 400 mg/L RBBR at different applied potential and 25℃ temperature.

Figure 10. Nyquist plots of 5CBD electrode in aqueous solution of 0.25 M H_2SO_4, 0.25 M Na_2SO_4 (pH 6.5) and 0.25 M KOH (pH 11) containing 400 mg/L RBBR (a) at oxidation potential, (b) at zero applied potential.

Figure 11. Nyquist plots of a consecutive runs (run number 30) in solution of 0.25 M H_2SO_4, 0.25 M Na_2SO_4 (pH 6.5) and 0.25 M KOH (pH 11) containing 400 mg/L RBBR at oxidation potential.

Figure 12. The effect of current density on (a) RBBR incineration and (b) COD removal with time over 5CBD electrode (the pH 3; the initial concentration of RBBR: 100 mg/L; volume: 100 mL; supporting electrolyte (Na_2SO_4) concentration: 0.25 M).

Fig. 1

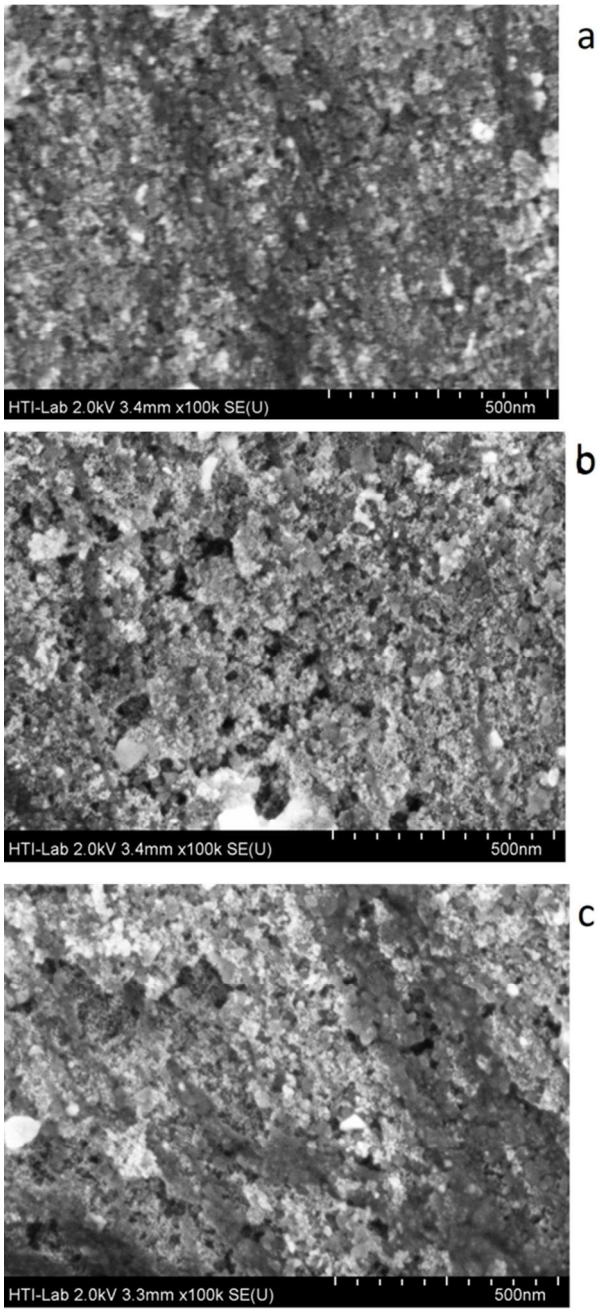

Fig. 2

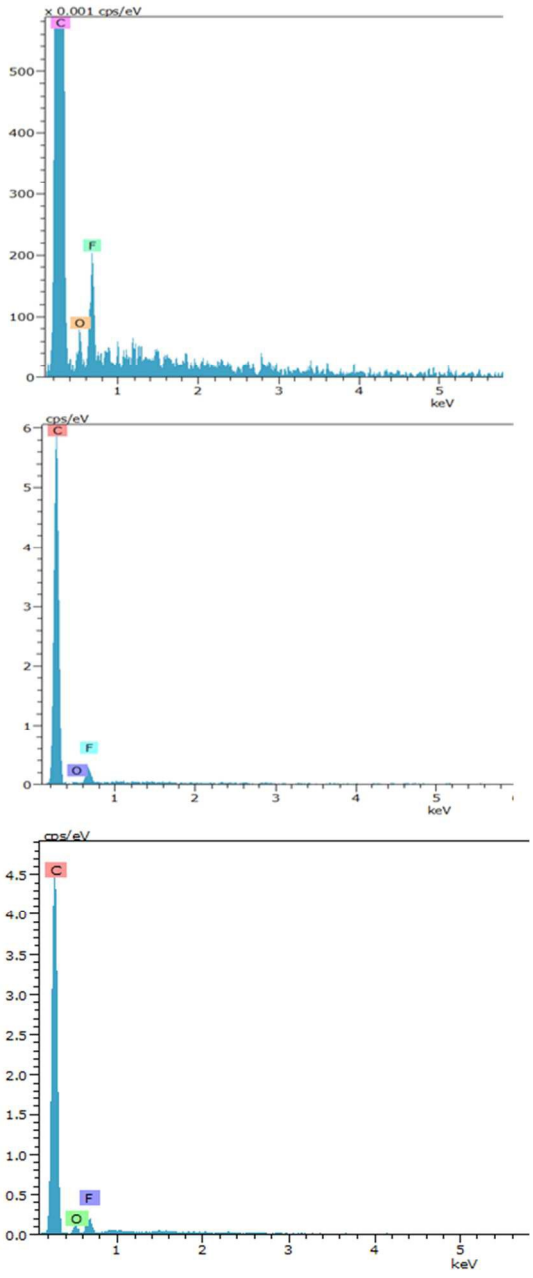

Fig. 3

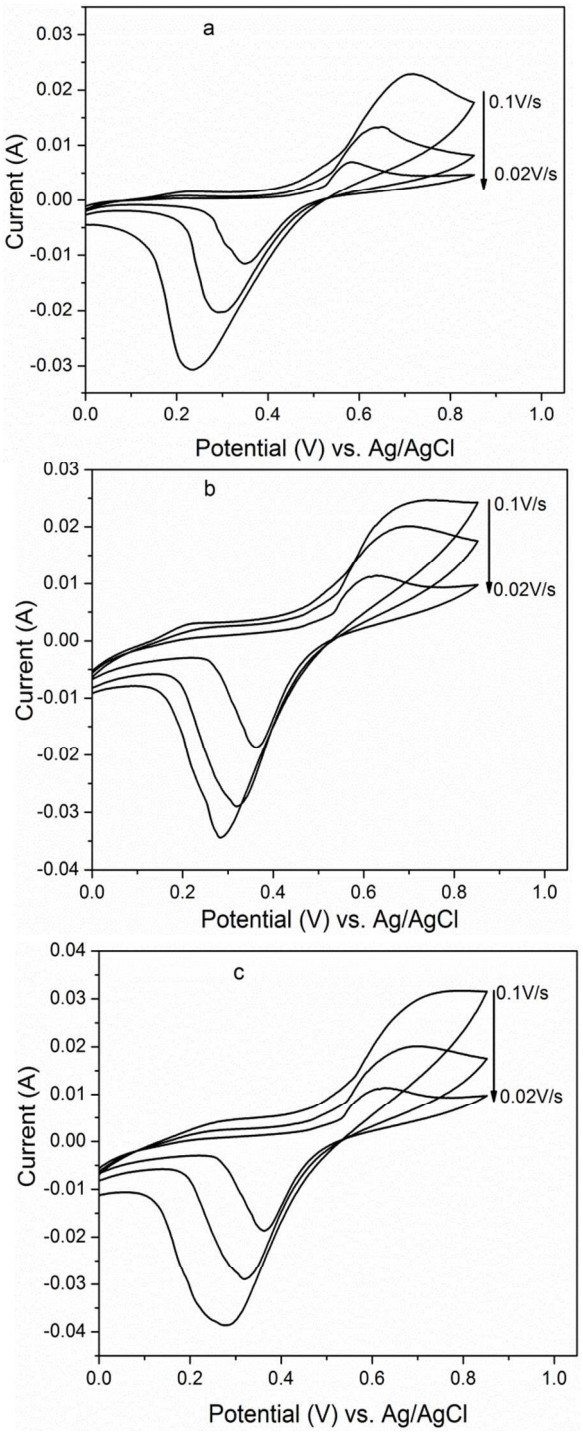

Fig. 4

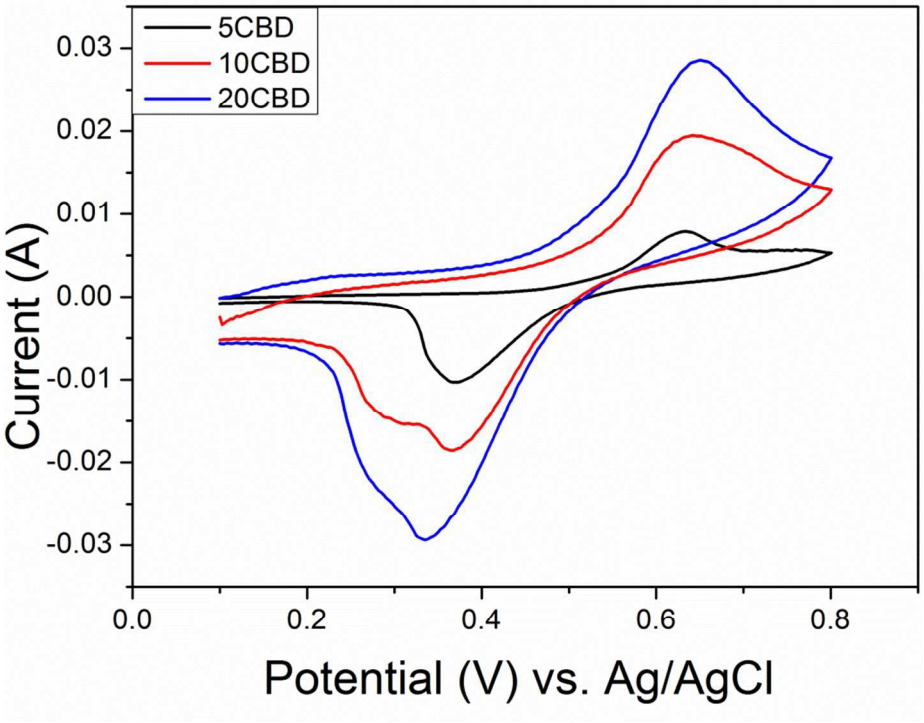

Fig. 5

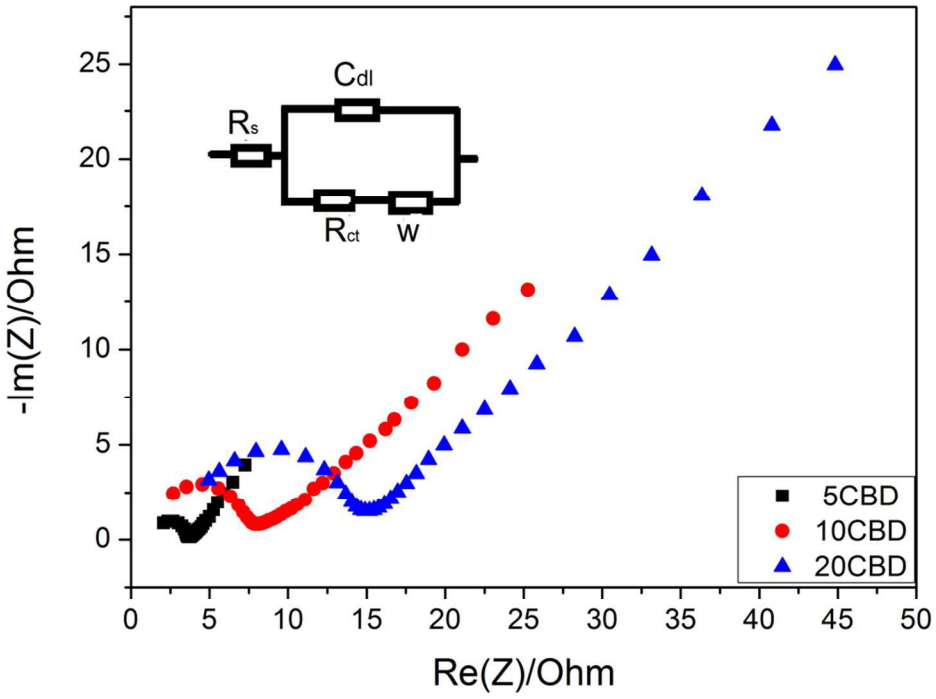

Fig.6

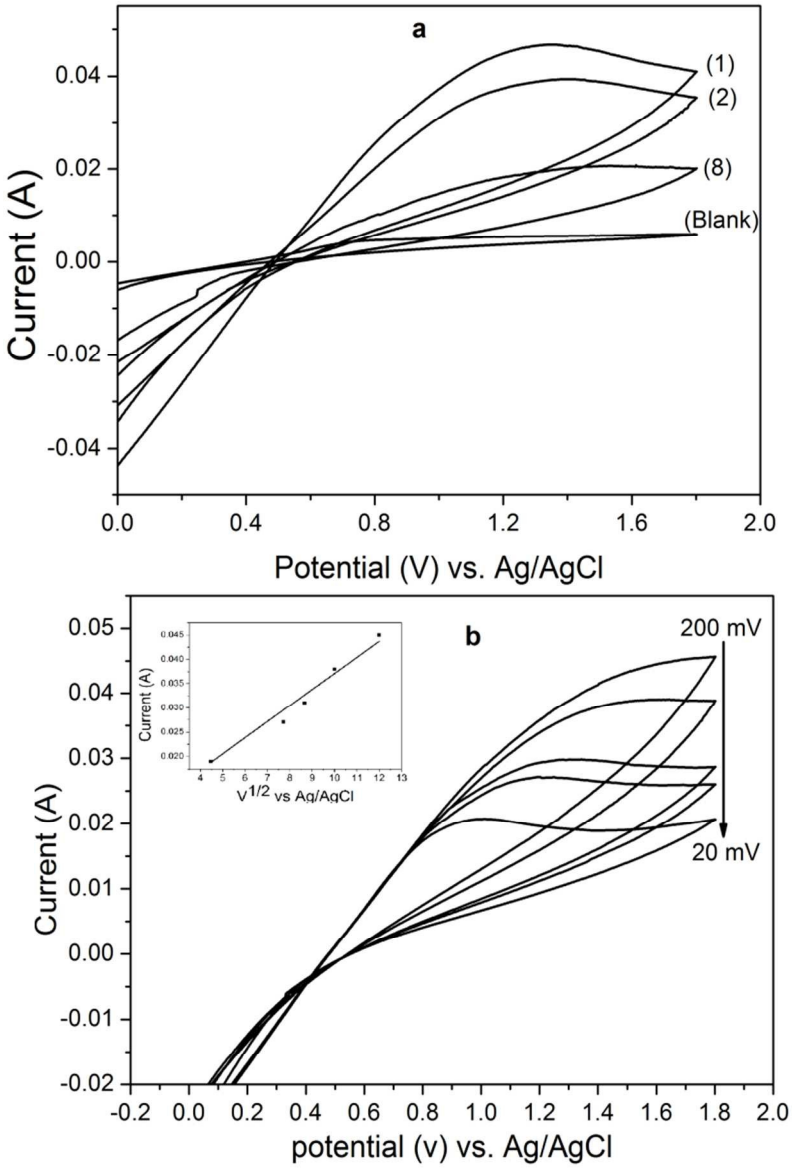

Fig. 7

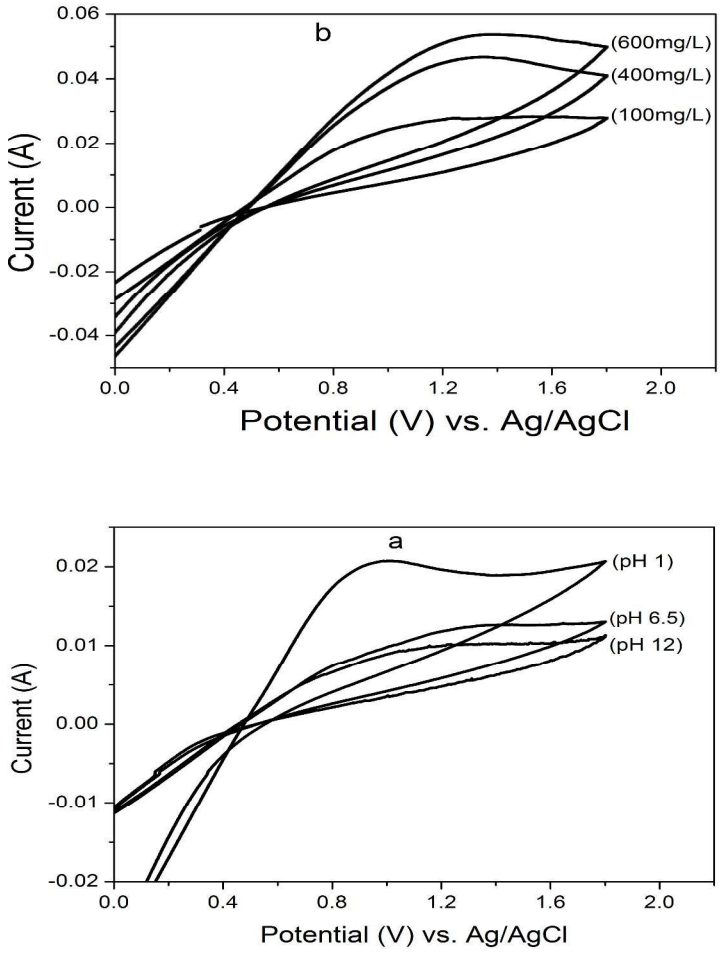

Fig. 8

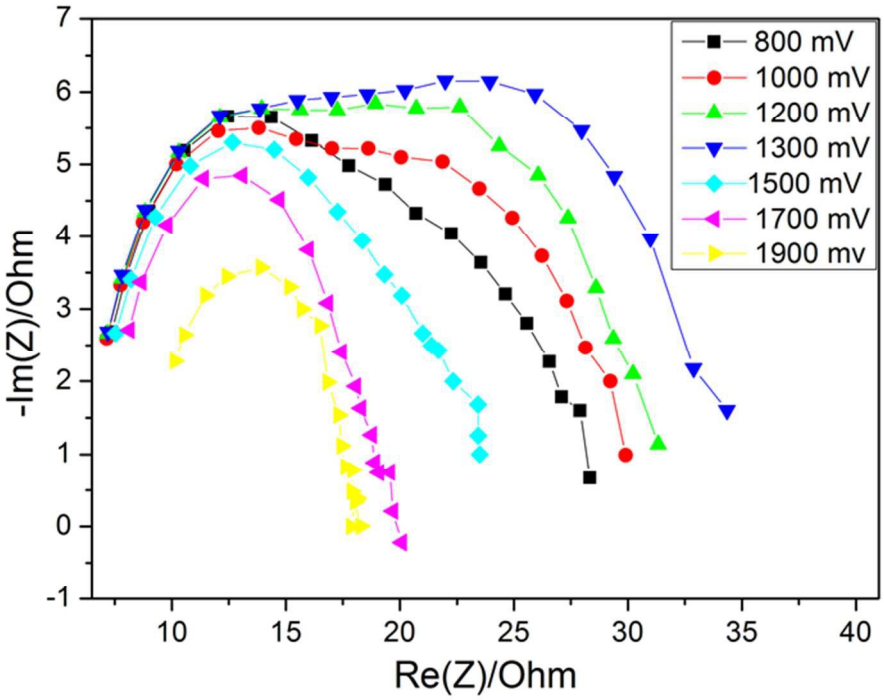

Fig. 9

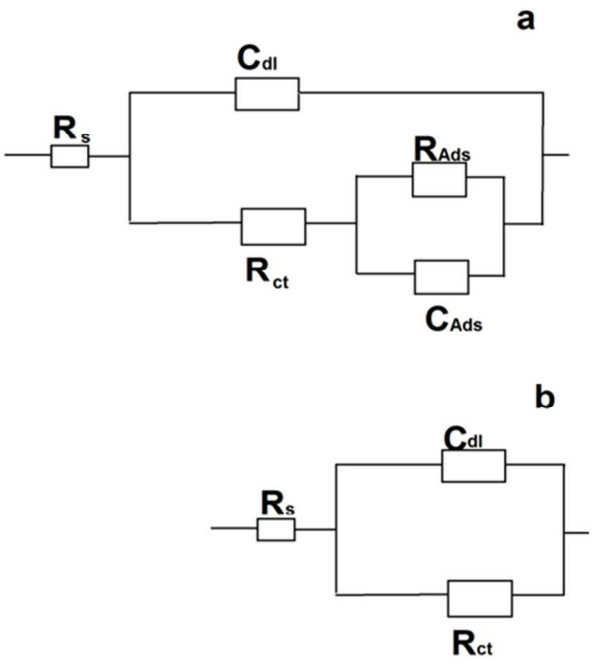

Fig 10

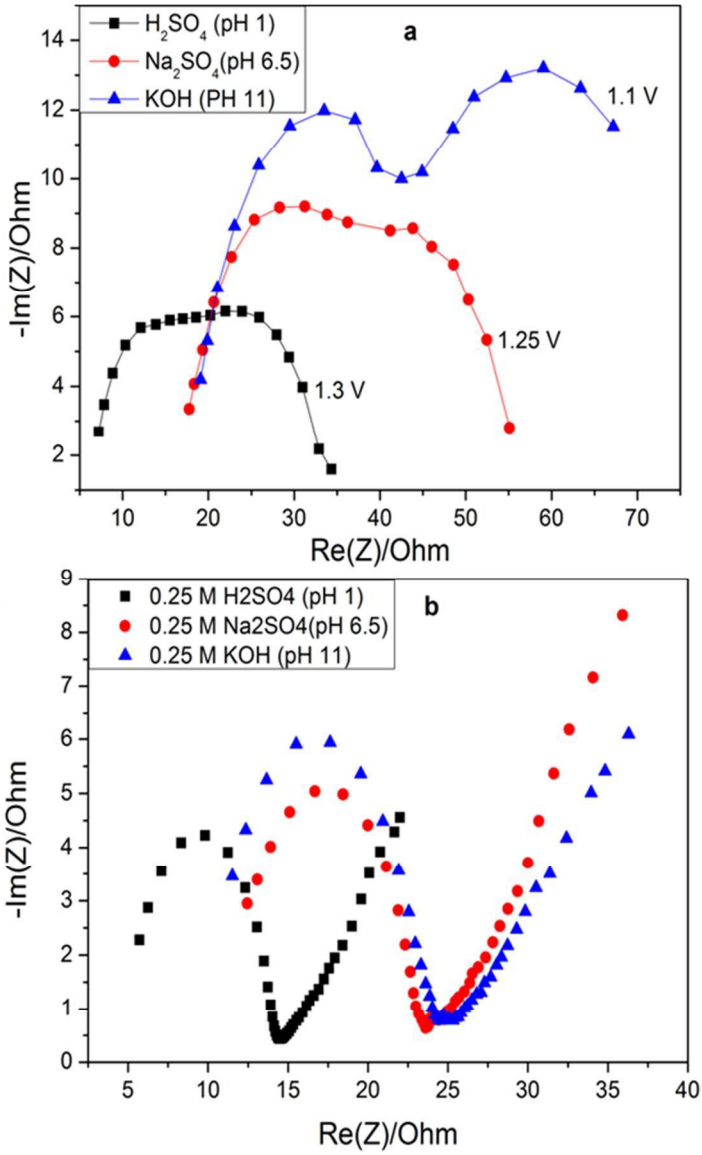

Fig. 11

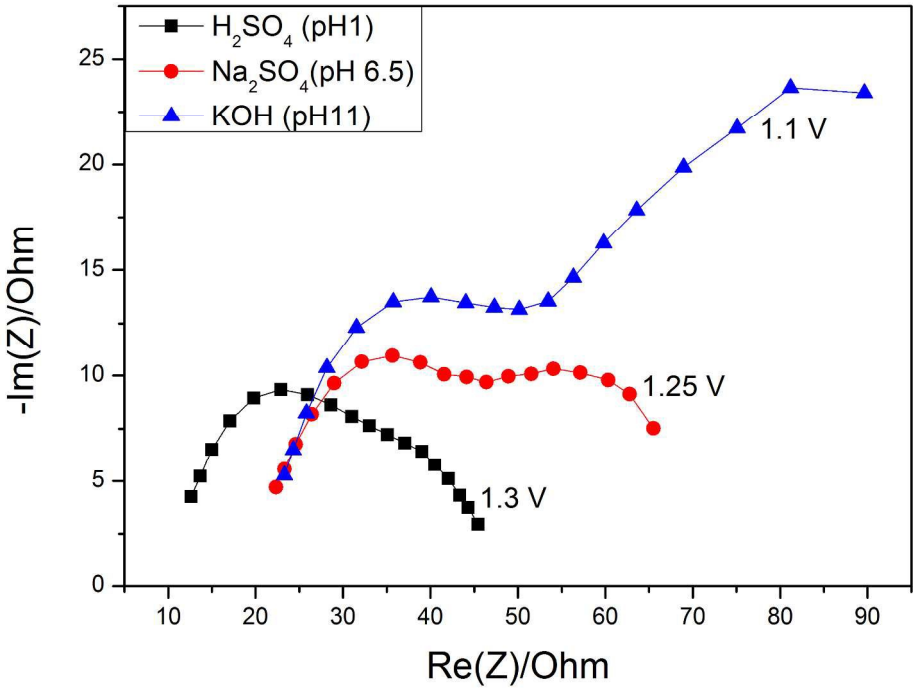

Fig. 12

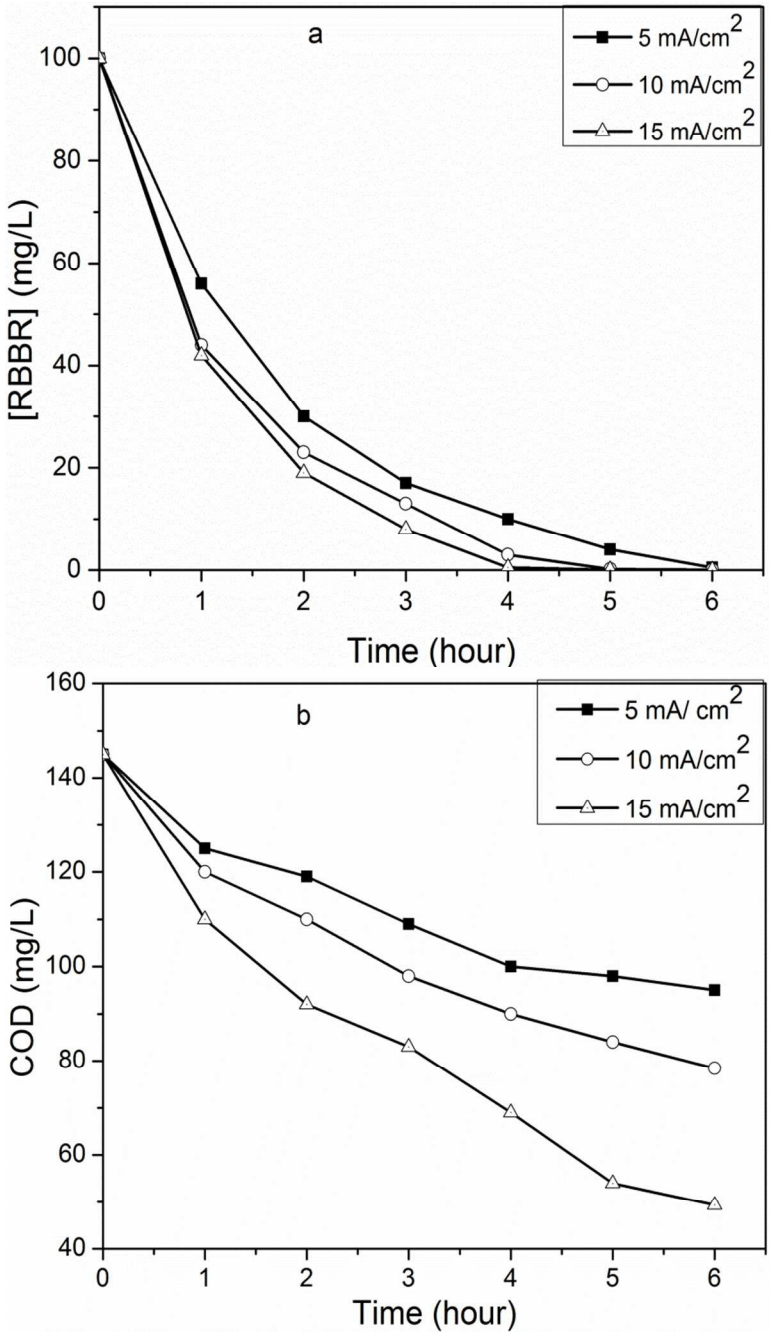

Tables:

Table 1. Electrochemical impedance data extracted from the Nyquist plots at different applied potential.

Potential mV	R_s (Ω cm^2)	R_{ct} (Ω cm^2)	C_{dl} (μF/cm^2)	R_{ads} (Ω cm^2)	C_{ads} (μF/cm^2)
900	6.88	11.98	0.700	8.835	15.11
1000	6.9	12.15	0.695	9.81	12.37
1200	6.908	12.5	0.679	11	10.72
1300	6.888	12.55	0.672	11.96	10.7
1500	7.1	11.25	0.653 7	4.998	18.28
1700	7.548	10.38	0.682		
1900	8.386	9.231	0.804		